

## Article

# Effect of United Expanding Admixture on Autogenous Shrinkage and Early Age Mechanical Properties of High-Strength Engineered Cementitious Composites

Ajad Shrestha <sup>1,\*</sup>, Nauman Ahmad <sup>1</sup> , Zhi Zhang <sup>1</sup>, Sanket Rawat <sup>2</sup>  and Lingzhi Li <sup>1</sup>

<sup>1</sup> Department of Disaster Mitigation for Structures, College of Civil Engineering, Tongji University, 1239 Siping Road, Shanghai 200092, China

<sup>2</sup> School of Engineering, Design and Built Environment, Western Sydney University, Penrith, NSW 2751, Australia

\* Correspondence: ajadsh1@tongji.edu.cn

**Abstract:** High-strength engineered cementitious composites (HS-ECCs) have garnered significant attention for their superior mechanical properties and ductility. However, their high autogenous shrinkage, caused by a low water-to-binder ratio, high cementitious content, and lack of coarse aggregate, often results in early-age cracking, limiting their broader use in civil engineering. Incorporating iron sand in HS-ECCs has enhanced their mechanical properties, reduced the carbon footprint, and moderately decreased shrinkage strain compared to traditional silica sand; however, the shrinkage strain remains substantial. This study aims to reduce the autogenous shrinkage of HS-ECCs further by incorporating united expanding admixtures (UEAs)—calcium oxide-based (CEA) and magnesium oxide-based (MEA) expansive agents—in varying amounts (3% to 10% by mass of cement). This study also examines the impact of these admixtures on the workability and mechanical properties of HS-ECCs. The results show that increasing the UEA content significantly reduces autogenous shrinkage strain, achieving a 40.66% reduction at 10% UEA, from 1007.31  $\mu\epsilon$  to 647.18  $\mu\epsilon$ . While higher UEA content decreases workability, as indicated by lower fluidity and penetration depth, the compressive strength remains largely unaffected. The tensile strength peaks at 12.38 MPa with 3% UEA but declines at higher contents, with higher UEA content effectively minimizing crack formation. The novelty of this research lies in the combined use of waste iron sand and UEA, optimizing the balance between workability, mechanical properties, and autogenous shrinkage reduction in HS-ECCs. These findings support the broader application of HS-ECCs in civil engineering projects requiring high mechanical properties and low shrinkage.

**Keywords:** high-strength engineered cementitious composite (HS-ECCs); united expanding admixture (UEA); autogenous shrinkage; workability; mechanical properties



**Citation:** Shrestha, A.; Ahmad, N.; Zhang, Z.; Rawat, S.; Li, L. Effect of United Expanding Admixture on Autogenous Shrinkage and Early Age Mechanical Properties of High-Strength Engineered Cementitious Composites. *Buildings* **2024**, *14*, 2868. <https://doi.org/10.3390/buildings14092868>

Academic Editors: Binsheng Zhang and Jan Fort

Received: 1 July 2024

Revised: 3 September 2024

Accepted: 9 September 2024

Published: 11 September 2024



**Copyright:** © 2024 by the authors. Licensee MDPI, Basel, Switzerland. This article is an open access article distributed under the terms and conditions of the Creative Commons Attribution (CC BY) license (<https://creativecommons.org/licenses/by/4.0/>).

## 1. Introduction

Engineered cementitious composites (ECCs) have received significant attention in the construction industry due to their superior tensile properties, including a tensile strength of 6–10 MPa and tensile strain greater than 3%, compared to ultra-high-performance concrete (UHPC) and conventional concrete [1,2]. Developed by Li [3] using the principles of micromechanics and fracture mechanics [3–5], ECCs are known for their strain-hardening properties and multi-cracking behavior [6,7], which contribute to enhanced energy absorption capacity and durability [7,8]. These properties make ECCs suitable for various applications, including pavement overlays, link slabs for bridge expansion joints, and repair material. Although ECCs possess significant tensile properties [9–12], they have low elastic modulus ( $E$ ) to cube compressive strength ( $f_{cu}$ ) ratios compared to traditional concrete, limiting their applications in real-world scenarios [13]. This low modulus results in reduced stiffness, making it challenging to use ECCs for constructing entire structural members. To

overcome this limitation, high-strength engineered cementitious composites (HS-ECCs) were developed, featuring enhanced mechanical properties, including a tensile strain capacity of more than 2% and a compressive strength exceeding 80 MPa [13,14]. HS-ECC preparation involves fundamental principles from UHPC, such as a low water-to-binder (w/b) ratio and the incorporation of ultra-fine particles, which enhance the microstructure and improve interfacial bonding and compressive strength [14]. The incorporation of ultra-high-molecular-weight polyethylene (PE) fibers further enhances the mechanical properties of HS-ECCs [5]. Optimal HS-ECC performance is achieved with w/b ratios of 0.13 to 0.24 and s/b ratios of 0.077 to 0.3, respectively [14].

Although HS-ECCs possess superior mechanical properties, their low water-to-binder (w/b) ratio, low sand-to-binder (s/b) ratio, and lack of coarse aggregate result in significant shrinkage strain. In civil engineering applications, shrinkage is mainly categorized into autogenous and drying shrinkage. While chemical and plastic shrinkages also occur, they are less significant in civil engineering applications due to their minimal stress impact. Autogenous shrinkage is particularly critical in HS-ECCs [15,16]. It occurs in sealed and isothermal conditions due to chemical reactions among internal raw materials without moisture loss to the surroundings [17,18]. Autogenous shrinkage can cause multiple cracks at an early stage, when the tensile strength is still developing, which negatively impacts the structure's durability and stiffness [15,16,18–20]. The formation of multiple cracks in HS-ECCs can relieve shrinkage stresses [21]. Autogenous shrinkage is measured from the final setting time (FST), which is when the cementitious material has fully solidified and hardened [21,22]. Ye et al. [21] observed that reducing the w/b ratio from 0.24 to 0.13 doubled the autogenous shrinkage in HS-ECCs, increasing from 6000 to 12,000  $\mu\epsilon$ . Chen et al. [22] reported an autogenous shrinkage strain of 1600  $\mu\epsilon$  for HS-ECCs with a 0.145 w/b ratio and 0.30 s/b ratio. This is significantly higher than the autogenous shrinkage strain of standard ECC, which is around 1000  $\mu\epsilon$  [19]. High autogenous shrinkage causes early cracking, which reduces the overall strength and durability of structures. To address these challenges, developing effective strategies to mitigate autogenous shrinkage is crucial for enhancing the practical applications of HS-ECCs in the construction industry.

Previous research has explored various methods to reduce autogenous shrinkage, such as shrinkage-reducing admixtures (SRAs), calcium sulfoaluminate (CSA) cement, superabsorbent polymers (SAPs), and united expansion agents (UEAs) [23–28]. Incorporating SRAs reduces capillary pores, thereby decreasing autogenous shrinkage. Chen et al. [22] reported a 15–27% reduction in HS-ECC shrinkage within 3 days, with minimal effects on compressive strength. Some researchers have utilized internal curing (IC) to reduce autogenous shrinkage. Zhang et al. [29] reported a 60% reduction in autogenous shrinkage by using pre-wetted sand, such as 0.18 mm zeolite, as an IC medium. Expansion agents may also help reduce autogenous shrinkage in HS-ECCs. However, the impact of such agents on the shrinkage behavior of HS-ECCs has yet to be thoroughly investigated, leaving a gap in the current understanding of how these additives influence the material's performance. Expansive products like ettringite and calcium hydroxide help minimize autogenous shrinkage by reducing capillary pores in the matrix. The crystallization and expansion pressures from macroscopic volume expansion partially counteract shrinkage stress, reducing the risk of cracking [27,29,30]. In addition to autogenous shrinkage, thermal shrinkage can cause cracks. These can be prevented by incorporating admixtures, such as phase-change materials, that counteract thermal stress [31]. Recent research has investigated replacing silica sand with iron sand in HS-ECCs, demonstrating an effective reduction in autogenous shrinkage and enhanced mechanical properties [32]. Iron sand, a byproduct of iron ore processing [33], poses environmental challenges due to its frequent disposal in landfills, rivers, or oceans [34]. In China alone, over 600 million tons of iron sand is produced annually, underscoring the need for sustainable utilization [35]. Using iron sand as a sustainable alternative to traditional sand can reduce waste and lower the carbon footprint of construction projects. Research has shown that incorporating iron sand enhances the mechanical properties of materials [36–38]. This approach to using iron sand

presents a novel strategy for mitigating shrinkage in HS-ECCs, warranting further exploration. Additionally, several studies have explored alternatives to river sand to promote sustainability [32,39,40].

While past research has primarily focused on enhancing the mechanical properties of HS-ECCs, mitigating shrinkage to promote its use in civil engineering applications has yet to be adequately studied. This study explores the innovative use of iron sand in HS-ECCs and provides a comprehensive analysis of additional methods to reduce autogenous shrinkage further. It specifically investigates the effects of incorporating UEA—both calcium-oxide-based expansive agent (CEA) and magnesium-oxide-based (MEA) expansive agents—through experimental investigation. Five mix proportions were prepared by replacing cement with UEA in different mass proportions (3%, 6%, 8%, and 10%). These were systematically tested to assess their effects on autogenous shrinkage, workability, and mechanical properties. This research aims to fill existing knowledge gaps and establish an experimental foundation for reducing significant autogenous shrinkage in HS-ECCs while balancing mechanical properties and workability, thereby promoting its application in civil engineering projects.

## 2. Research Significance

Autogenous shrinkage in HS-ECCs is a critical issue that leads to early-age cracking, restricting its practical applications. This high autogenous shrinkage primarily results from the low water-to-binder ratio ( $w/b$ ) and sand-to-binder ratio ( $s/b$ ), essential for achieving high mechanical properties and pseudo-strain-hardening behavior. Literature reviews reveal a significant gap in studies on the impact of UEA on autogenous shrinkage in HS-ECCs. Although incorporating iron sand in HS-ECCs reduces the carbon footprint, enhances mechanical properties, and mitigates autogenous shrinkage, shrinkage values remain relatively high.

This research aims to further reduce autogenous shrinkage in HS-ECCs, promoting the use of iron sand, which otherwise acts as a pollutant. This study seeks to develop a balanced HS-ECC mixture by incorporating UEA with iron sand to optimize the mechanical performance while controlling autogenous shrinkage. This balanced mixture is intended to enhance the practicality of HS-ECCs for real-world applications, including seismic-resistant structures, bridge and tunnel construction, and high-performance buildings.

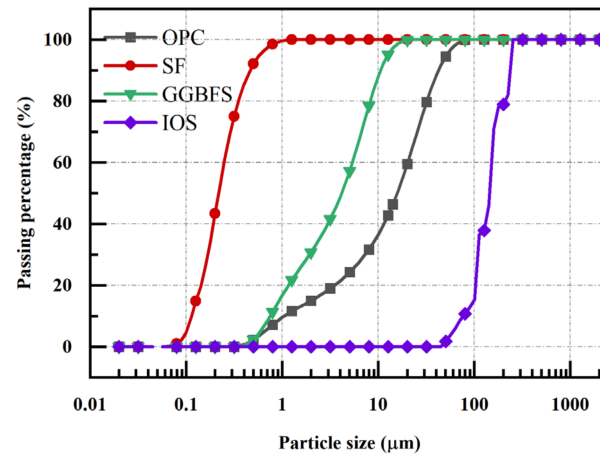
## 3. Experimental Programs

### 3.1. Raw Materials

The raw materials used in this study included ordinary Portland cement (OPC) 52.5R, ground granulated blast furnace slag (GGBFS), silica fume (SF), iron sand (IOS), and high-range water-reducing admixtures (HRWRAs). SF and GGBFS were added to promote secondary hydration, which enhances the mechanical properties. A summary of oxide compositions is presented in Table 1. Iron sand with a particle size of 80–120 mesh was used for better fiber dispersion. Using iron sand instead of river sand benefits the environment [30] as it is a waste product from the iron industry [31,32]. Incorporating iron sand as an aggregate in HS-ECCs can reduce waste and positively impact the environment while simultaneously enhancing mechanical properties [33]. Figure 1 illustrates the particle size distribution of the binder and iron sand. Ultra-high-molecular-weight polyethylene (PE) fibers, with a length of 18 mm and a diameter of 24  $\mu\text{m}$ , were used. The properties of the fibers used in preparing HS-ECCs are detailed in Table 2. HRWRA was utilized to maintain workability. UEA, which is a combination of CEA and MEA, was incorporated by partially replacing cement by mass in the mixture.

**Table 1.** Oxide compositions of binders and UEA.

Materials	Na <sub>2</sub> O	MgO	Al <sub>2</sub> O <sub>3</sub>	SiO <sub>2</sub>	P <sub>2</sub> O <sub>5</sub>	SO <sub>3</sub>	K <sub>2</sub> O	CaO	TiO <sub>2</sub>	MnO	Fe <sub>2</sub> O <sub>3</sub>
OPC	0.51	5.28	8.32	20.69	0.11	3.79	1.00	54.82	0.56	0.15	4.77
GGBS	<0.01	11.89	18.64	29.91	0.06	3.77	0.45	32.71	1.28	0.55	0.74
SF	1.03	1.30	1.16	91.68	0.23	0.48	2.90	0.72	<0.01	0.04	0.46
IOS	0.75	1.42	2.56	6.00	0.22	0.02	0.14	0.82	9.95	0.47	76.72
CEA	<0.01	1.13	1.68	2.91	<0.01	0.79	<0.01	89.90	<0.01	<0.01	3.59
MEA	<0.01	92.59	0.59	3.28	<0.01	0.09	<0.01	2.16	<0.01	<0.01	1.29

**Figure 1.** Particle size distribution curves.**Table 2.** Properties of fibers.

Diameter (μm)	Length (mm)	Tensile Strength (MPa)	Elastic Modulus (GPa)	Density (g/m <sup>3</sup> )	Elongation (%)
24	18	2900	116	0.97	2.5

### 3.2. Mix Proportions

Table 3 illustrates the mix proportions of HS-ECCs with various UEA contents. The UEA contents were 3%, 6%, 8%, and 10% by mass of cement, with CEA and MEA added in equal proportions by mass. The mixes are labelled as “ECC-U-3”, for example, which denotes HS-ECCs with a total UEA content of 3%, consisting of 1.5% CEA and 1.5% MEA. HRWRA was maintained at a constant dosage of 10 g/L, and PE fibers were kept at a 1.8% volume proportion.

**Table 3.** Mix proportions of HS-ECCs (mass ratio).

Mix ID	OPC	GGBFS	SF	IOS	Water	PE (Vol %)	UEA (Mass %)
ECC-U-0	1.00	1.20	0.30	0.80	0.30	1.8	0
ECC-U-3	0.97	1.20	0.30	0.80	0.30	1.8	3
ECC-U-6	0.94	1.20	0.30	0.80	0.30	1.8	6
ECC-U-8	0.92	1.20	0.30	0.80	0.30	1.8	8
ECC-U-10	0.90	1.20	0.30	0.80	0.30	1.8	10

### 3.3. Mixing Procedure

The mixing procedure was divided into two parts: dry material mixing and fiber mixing, as shown in Figure 2. After adding water and HRWR, cementitious material was blended with sand at 140 rpm for 10 min. After achieving fluid consistency, PE fibers were

added and mixed at 420 rpm until there were no dry fibers or fiber lumps. The mixing procedure was adopted to maintain proper dispersion throughout the mixture.

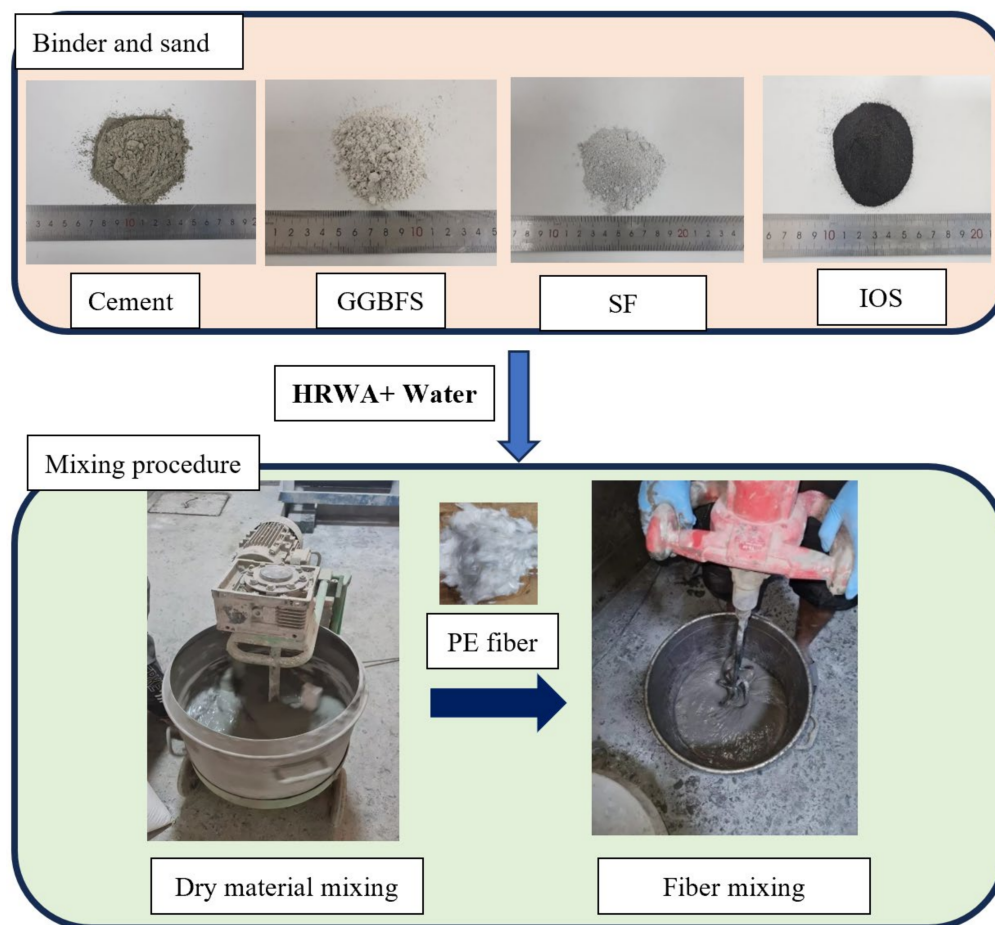


**Figure 2.** Mixing procedure.

### 3.4. Testing Procedure

The experimental investigation included evaluating autogenous shrinkage, workability, and mechanical properties. Mechanical properties were assessed through cube compressive strength and direct tensile tests using specimens with a fiber volume fraction of 1.8%. Workability was evaluated using penetration depth and fluidity tests with fiber-free specimens. Similarly, assessments of autogenous shrinkage and setting times were conducted on fiber-free specimens. Three samples were prepared for each mixture to ensure reliability and repeatability. Standard deviations and means were calculated to assess variability and central tendency, respectively. Furthermore, detailed statistical analysis was conducted to examine the relationship between UEA content and the tested properties, providing insights into how varying UEA levels affect the performance characteristics of HS-ECCs.

#### 3.4.1. Setting Times

The setting times of the HS-ECC mixtures were determined using a Vicat apparatus following the Chinese standard GB/T 1346-2011 [41] as shown in Figure 3. Each mixture was placed into a conical mold with a bottom diameter of  $75 \text{ mm} \pm 0.5 \text{ mm}$  and a top diameter of  $65 \text{ mm} \pm 0.5 \text{ mm}$ . The initial setting time (IST) was assessed 30 min after the addition of water to the mixture. The IST is defined as the point at which the needle of the Vicat apparatus penetrates to a depth of  $4 \text{ mm} \pm 1 \text{ mm}$  from the base of the mold. Following the IST measurement, the mold was rotated 180 degrees to measure the final setting time (FST). The FST was determined using a specialized FST needle and was considered reached

when the needle left no impression on the mold's surface. Three samples were prepared for each mix proportion to ensure the reliability of the results.



Figure 3. Setting times.

### 3.4.2. Autogenous Shrinkage Test

For measuring autogenous shrinkage, corrugated plastic tubes with a length of  $420 \pm 5$  mm and an outer diameter of  $29 \text{ mm} \pm 0.5$  mm were utilized [42] as shown in Figure 4. The mixture was poured carefully into the tubes while on a vibrating table to avoid air entrapment. The tubes were clamped to prevent extension of length. Three specimens were prepared for each mix to ensure accuracy and repeatability. The specimens were set in the testing machine 15 min before the FST, with the initial measurement taken from the FST. The specimens were cured in a standard curing box with a temperature of  $23 \pm 2$  °C and a relative humidity of 95%. The readings were automatically recorded by the machine every 30 min. The autogenous shrinkage of the specimen at time 't' was calculated using the following equation:

$$\varepsilon_{as}(t) = \frac{\Delta L(t)}{L(t_{fs}) - 2 \cdot L_{plug}} = \frac{(L(t_{fs}) - 2 \cdot L_{plug}) - (L(t) - 2 \cdot L_{plug})}{L(t_{fs}) - 2 \cdot L_{plug}} = \frac{L(t_{fs}) - L(t)}{L(t_{fs}) - 2 \cdot L_{plug}} \quad (1)$$

where  $\varepsilon_{as}(t)$  is the autogenous shrinkage of specimen at time  $t$ ,  $t$  is the elapsed time from the final setting time,  $t_{fs}$  is the final setting time of specimen,  $\Delta L(t)$  is the length change of specimen at time  $t$ ,  $L(t_{fs})$  and  $L(t)$  are the lengths of the specimen at time  $t_{fs}$  and  $t$ , respectively, and  $L_{plug}$  is the length of the end plug.

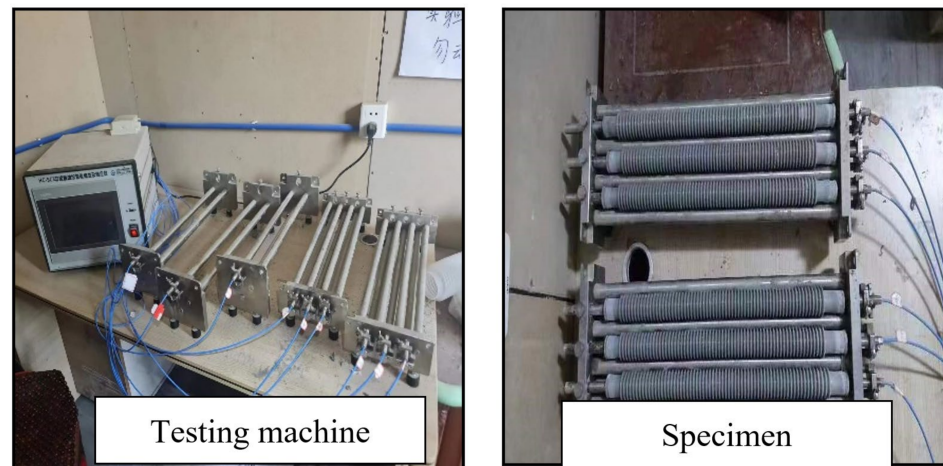


**Figure 4.** Autogenous shrinkage tests.

### 3.4.3. Apparent Density Test

The apparent density test [43] measures the mass per unit volume of the mortar. The density of the matrix was determined using a one-liter cylindrical bucket with a diameter of 108 mm and a height of 109 mm. Figure 5a shows the experimental setup for apparent density test. This test was conducted immediately after the mixing procedure was completed to ensure the results reflected the fresh state of the mortar. To ensure accuracy and consistency, three specimens were prepared for each mix proportion.

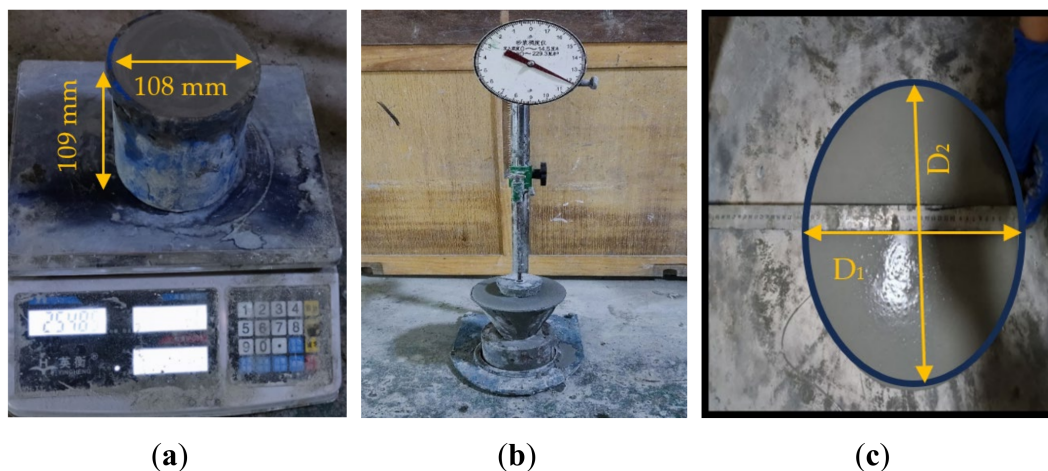


**Figure 5.** (a) Apparent density test; (b) penetration depth test; (c) fluidity test.

### 3.4.4. Penetration Depth and Fluidity Test

For the penetration depth test, the mixture was poured into an inverted vessel and compacted using a steel rod with a diameter of 10 mm and a length of 350 mm, featuring a rounded end [43], as shown in Figure 5b. Following compaction, the test cone's tip was brought into contact with the surface of the mixture. The screw was then loosened, allowing the test cone to fall and penetrate the mixture for 10 s. The penetration depth was measured as the difference between the final reading and the initial reading. Three samples were prepared for each mix proportion to ensure consistent results. For the fluidity test [44], the mixture was poured into a cone with a height of  $60 \text{ mm} \pm 0.5 \text{ mm}$ , a top inner diameter of  $70 \text{ mm} \pm 0.5 \text{ mm}$ , a bottom inner diameter of  $100 \text{ mm} \pm 0.5 \text{ mm}$ , and a wall thickness of 5 mm as shown in Figure 5c. The initial measurement was taken 30 s after lifting the cone, which was carefully lifted vertically to avoid disturbance. The diameters of both sides were taken as a measurement. This test was performed immediately after the

completion of the mixing procedure. Three tests were conducted for each mix proportion to ensure repeatability.

### 3.4.5. Cube Compressive Strength Test

To determine the cube compressive strength ( $f_{cu}$ ), a cube with dimensions of 100 mm × 100 mm × 100 mm was loaded at a rate of 10 kN/s [45]. Three cubes were prepared for each mixture and cured in a standard curing box at a temperature of  $20 \pm 5$  °C and relative humidity of 95% for 7 days. Before testing, the dimensions of the cubes were measured to ensure a precise calculation of the cube compressive strength.

### 3.4.6. Direct Tensile Test

JSCE specifications [46] were followed to assess the tensile capacity of the material. Dog bone-shaped specimens were used to determine the tensile strength ( $f_t$ ) and tensile strain ( $\epsilon_t$ ). Three dog bone specimens were prepared to determine the 7-day tensile strength ( $f_t$ ) and tensile strain ( $\epsilon_t$ ). The dimensions of the dog bone specimen are shown in Figure 6b. The specimens were cured in a standard curing box at a temperature of  $20 \pm 5$  °C and a relative humidity of 95% for 7 days. Two linear variable displacement transducers (LVDTs) were used to determine the deformation. The specimen was loaded at 0.5 mm/min and changed to 1 mm/min after the initial crack.

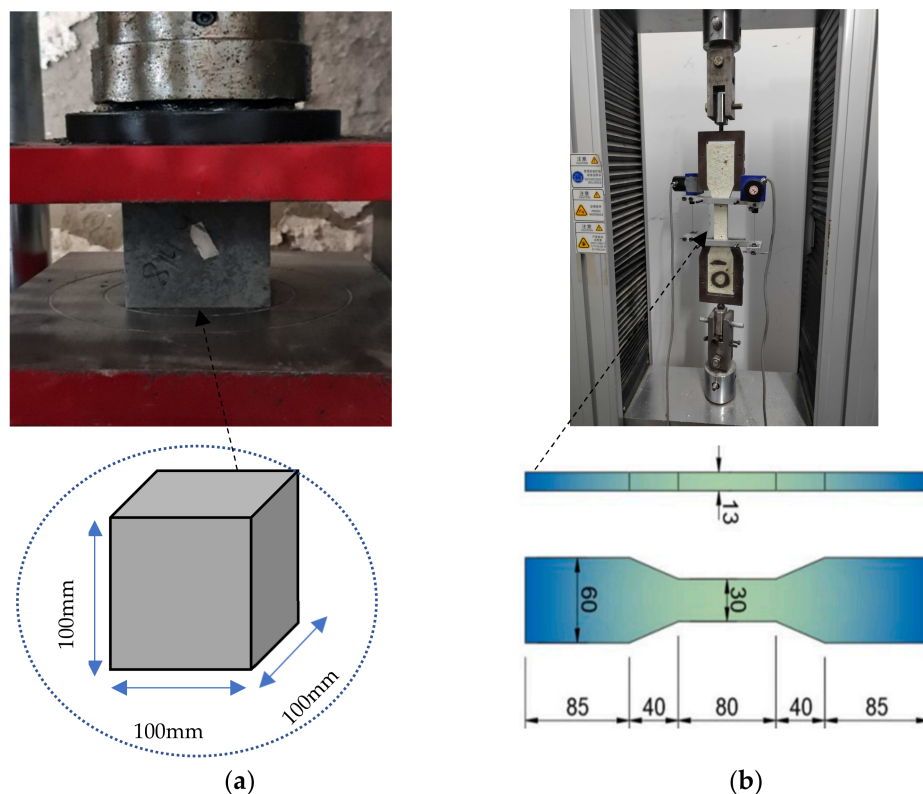


**Figure 6.** (a) Cube compressive strength test; (b) direct tensile test.

## 4. Results and Discussion

### 4.1. Setting Times

The setting times of HS-ECCs, both IST and FST, consistently decreased as UEA content increased. This reduction can be attributed to the reactions between CEA and MEA with water, forming calcium hydroxide ( $\text{Ca}(\text{OH})_2$ ) and magnesium hydroxide ( $\text{Mg}(\text{OH})_2$ ), respectively. These reactions accelerate the hydration process. Additionally, the exothermic nature of these chemical reactions releases heat, raising the temperature of the cement paste, which further accelerates hydration [47], thus reducing the setting times.

The reference mixture without UEA showed an IST of 423 min and an FST of 533 min. With the addition of 3% UEA, the IST decreased to 375 min and the FST to 450 min. Higher contents of UEA resulted in even shorter setting times, with the mixture containing 10% UEA exhibiting an IST of 251 min and an FST of 302 min. Table 4 provides a summary of setting time results

**Table 4.** Summary of setting time results.

Samples	Initial Setting Time (min)	Final Setting Time (min)
ECC-U-0	423 ( $\pm 24.54$ )	533 ( $\pm 23.37$ )
ECC-U-3	375 ( $\pm 4.08$ )	450 ( $\pm 14.14$ )
ECC-U-6	356 ( $\pm 17.28$ )	431 ( $\pm 20.05$ )
ECC-U-8	300 ( $\pm 25.49$ )	370 ( $\pm 10.80$ )
ECC-U-10	251 ( $\pm 16.08$ )	302 ( $\pm 13.59$ )

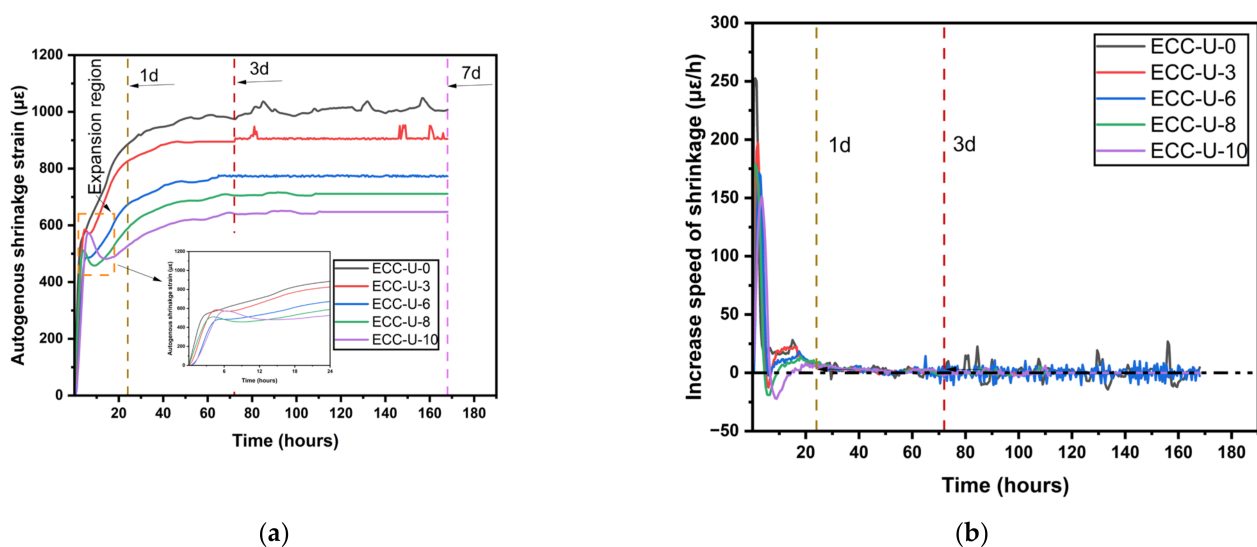
This demonstrates that increasing UEA content significantly accelerates the setting times, potentially expediting construction schedules. However, it may also reduce workability, complicating the use of HS-ECCs in civil engineering projects. Therefore, it is crucial to carefully select the appropriate UEA content to ensure a balance between setting times and workability, meeting all necessary performance requirements.

#### 4.2. Autogenous Shrinkage

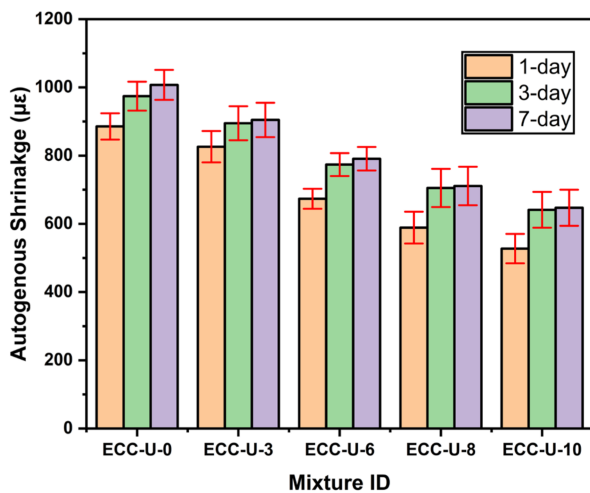
Figure 7a illustrates the impact of UEA on the autogenous shrinkage of HS-ECCs. Autogenous shrinkage measurement started from the FST to exclude the effects of chemical and plastic shrinkages, which have a minimal impact on civil engineering works. The results show a significant reduction in autogenous shrinkage with the increasing UEA content.

Figure 7b indicates that during the first 24 h, the shrinkage strain increased rapidly, and, thereafter, the rate of increase stabilized, approaching nearly zero after three days. The expansive nature of UEA is particularly evident within the initial 24 h. Measurements continued up to seven days, as no substantial changes in autogenous shrinkage were observed beyond this period.

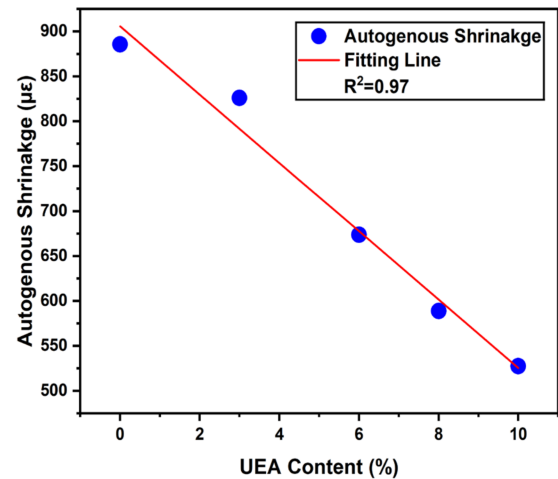
The ultimate shrinkage strain at seven days for the mixture without UEA was  $1007.31 \mu\epsilon$ . This value decreased to  $904.59 \mu\epsilon$  with a 3% UEA content. Further increases in UEA content to 6%, 8%, and 10% resulted in significant reductions in autogenous shrinkage, with strains of  $790.80 \mu\epsilon$ ,  $710.99 \mu\epsilon$ , and  $647.18 \mu\epsilon$ , respectively.



**Figure 7.** Cont.



(c)



(d)

**Figure 7.** (a) Autogenous shrinkage strains; (b) increased speed of shrinkage strains; (c) ultimate shrinkage strains; (d) relationship between autogenous shrinkage and UEA content.

The reduction percentages in autogenous shrinkage were notable: 11.59% at 3% UEA, 24.45% at 6% UEA, 33.46% at 8% UEA, and 40.66% at 10% UEA. These findings confirm that UEA effectively mitigates autogenous shrinkage in HS-ECCs. Table 5 provides a summary of the autogenous shrinkage results.

**Table 5.** Summary of autogenous shrinkage results.

Samples	Autogenous Shrinkage (µε)			Reduction in Autogenous Shrinkage (%)		
	1-Day	3-Day	7-Day	1-Day	3-Day	7-Day
ECC-U-0	885.62 (±31.52)	974.42 (±34.68)	1007.31 (±35.85)	Ref	Ref	Ref
ECC-U-3	826.07 (±37.55)	894.90 (±40.68)	904.59 (±41.12)	6.72	8.98	11.59
ECC-U-6	673.62 (±23.97)	773.78 (±27.53)	790.80 (±28.14)	23.94	22.66	24.45
ECC-U-8	588.88 (±38.16)	705.26 (±45.71)	710.99 (±46.08)	33.50	30.39	33.46
ECC-U-10	527.39 (±35.25)	641.16 (±42.85)	647.18 (±43.25)	40.45	37.63	40.66

A clear linear trend is observed between UEA percentage and autogenous shrinkage strain, as illustrated in Figure 7d. The scatter plot shows the experimental data points, with UEA content on the *x*-axis and autogenous shrinkage strain on the *y*-axis. The red line represents the best-fit linear regression, which has a high linear regression coefficient ( $R^2$ ) of 0.97, indicating a strong correlation. The equation of the fitting curve is as follows:

$$\text{Autogenous shrinkage strain} = -38.03 \times \text{UEA\%} + 905.69 \quad (2)$$

The reduction in autogenous shrinkage is primarily attributed to UEA's expansive reactions. These reactions produce hydration products that occupy a larger volume, thereby balancing the shrinkage and maintaining the matrix's overall volume stability. Additionally, UEA modifies the pore structure, reducing capillary tension and densifying the microstructure, contributing to the decreased autogenous shrinkage.

This reduction in autogenous shrinkage can enhance the practical application of HS-ECCs by decreasing the likelihood of early-stage cracking, thereby improving long-term durability.

#### 4.3. Apparent Density

It was observed that the apparent density remained essentially unchanged with varying contents of UEA, although a slight increase was noted as the UEA content increased. This increase in density can be attributed to the expansive reactions of CEA and MEA with water, which reduce porosity and create a denser cement matrix. Table 6 and Figure 8a illustrate the apparent density across different UEA contents. The highest density was recorded for the mixture with 10% UEA, falling within the normal concrete density range of  $1950 \text{ kg/m}^3$  to  $2800 \text{ kg/m}^3$ .

**Table 6.** Summary of density, fluidity, and penetration depth results.

Samples	Density ( $\text{kg/m}^3$ )	Flow Diameter (mm)	Penetration Depth (mm)
ECC-U-0	2434.56 ( $\pm 15.84$ )	357.50 ( $\pm 5.04$ )	11.20 ( $\pm 0.42$ )
ECC-U-3	2485.24 ( $\pm 10.30$ )	340.00 ( $\pm 3.56$ )	10.20 ( $\pm 0.49$ )
ECC-U-6	2515.02 ( $\pm 6.03$ )	325.50 ( $\pm 3.19$ )	9.50 ( $\pm 0.22$ )
ECC-U-8	2558.37 ( $\pm 11.01$ )	318.00 ( $\pm 5.89$ )	9.00 ( $\pm 0.57$ )
ECC-U-10	2594.68 ( $\pm 33.35$ )	310.00 ( $\pm 4.08$ )	8.30 ( $\pm 0.22$ )

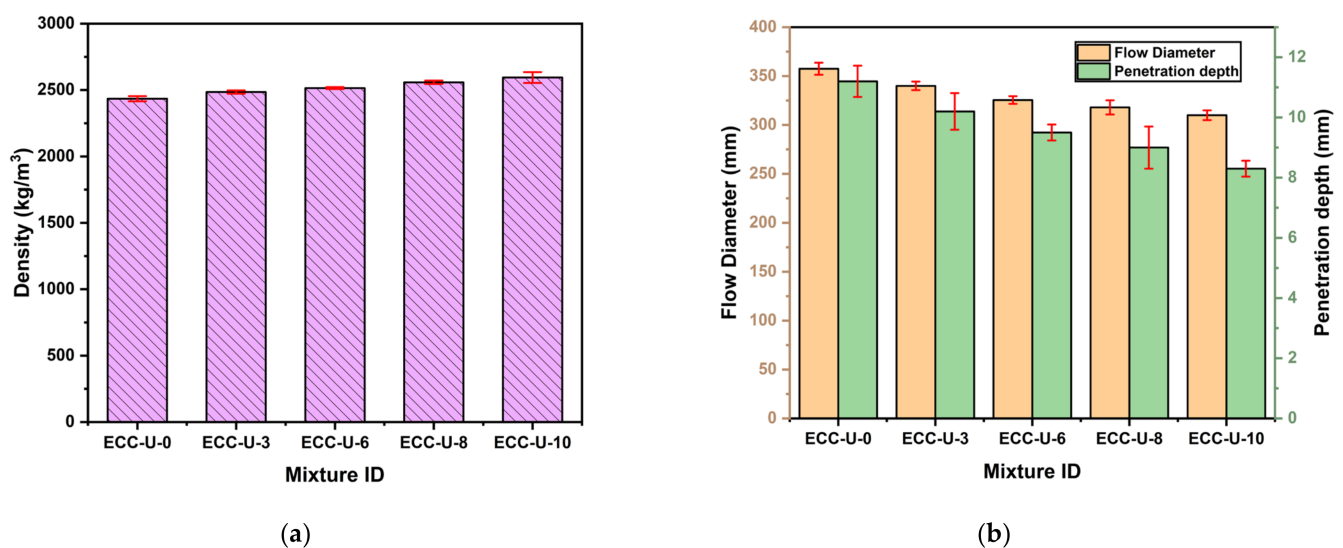


**Figure 8.** (a) Apparent densities; (b) flow diameters and penetration depths.

Since the apparent density of HS-ECCs with UEA falls within the normal concrete density range, it implies that HS-ECCs are suitable for construction applications.

#### 4.4. Fluidity and Penetration Depth

Workability was assessed using fluidity and penetration depth tests. Figure 8b and Table 6 illustrate the penetration depth and fluidity test experimental results with varying UEA contents. With a small content of UEA, a slight increase in workability may occur due to the expansive reaction, which reduces the internal friction and enhances the flowability. However, workability significantly decreases with a further increase in the UEA content, which is proven through flow diameter and penetration depth tests. This phenomenon is attributed to the accelerated hydration and densification caused by the expansive reaction of UEA, resulting in a more viscous and less workable matrix. It was observed that the mixture without UEA had the highest flow diameter and penetration depth of 357.5 mm and

11.2 mm, respectively. With an increase in UEA content, there were significant decreases in flow diameter and penetration depth, reaching 310 mm and 8.3 mm, respectively, at 10% UEA.

The decrease in workability caused by higher UEA content will affect its practical application in civil engineering. To ensure that HS-ECCs remain usable, their workability must be kept within acceptable limits. Therefore, it is crucial to either choose an optimal amount of UEA or adjust the mix proportions to achieve a balance between mechanical properties, workability, and shrinkage strain.

#### 4.5. Cube Compressive Strength

Figure 9a and Table 7 illustrate the impact of UEA content on the compressive strength of HS-ECCs after seven days. The data indicate that the addition of UEA has a negligible influence on compressive strength. Specifically, at the 7-day mark, the compressive strength of the mixture without UEA was 98.58 MPa, which increased to 99.43 MPa at a 3% UEA content. It further increased to 101.68 MPa at a UEA content of 6%. This slight increase in compressive strength with a higher UEA content is likely due to the formation of a denser cement matrix resulting from the reaction of an expansive admixture.

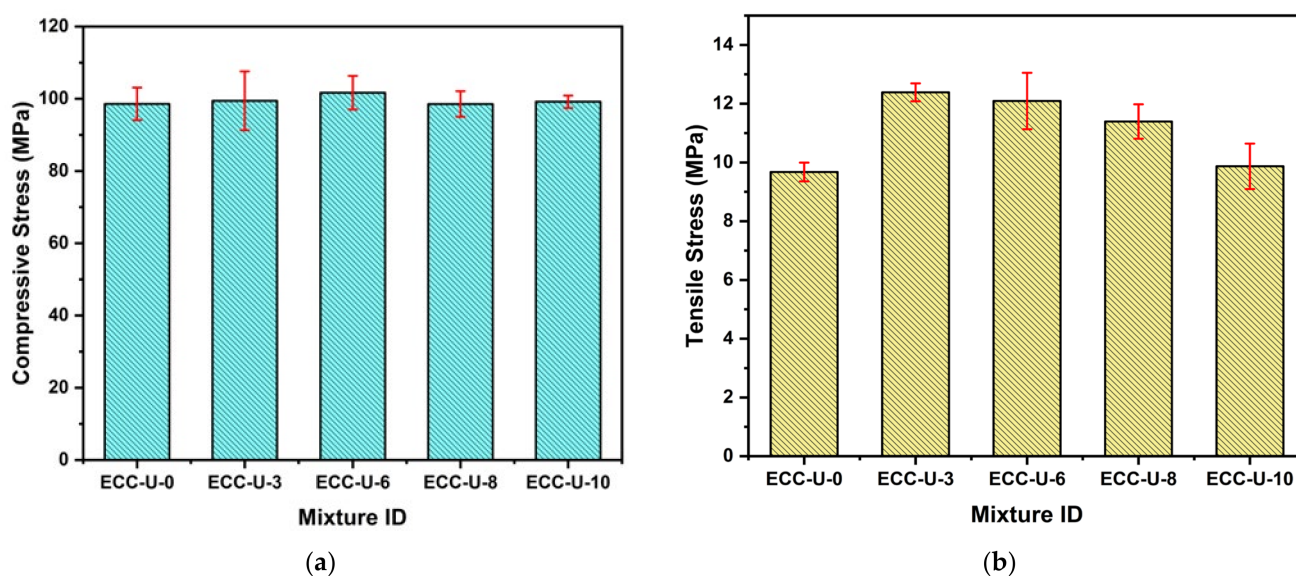


Figure 9. (a) Compressive strengths at 7 days; (b) tensile strengths at 7 days.

Table 7. Summary of mechanical property test results.

Samples	$f_{cu}$ (MPa)	$f_t$ (MPa)	$\epsilon_t$ (%)	Number of Cracks (Nc)
ECC-U-0	98.58 ( $\pm 3.69$ )	9.67 ( $\pm 0.26$ )	8.62 ( $\pm 1.52$ )	34 ( $\pm 2.83$ )
ECC-U-3	99.43 ( $\pm 6.65$ )	12.38 ( $\pm 0.25$ )	6.80 ( $\pm 0.51$ )	30 ( $\pm 5.09$ )
ECC-U-6	101.68 ( $\pm 3.80$ )	12.09 ( $\pm 0.78$ )	5.43 ( $\pm 0.32$ )	22 ( $\pm 4.32$ )
ECC-U-8	98.56 ( $\pm 2.90$ )	11.93 ( $\pm 0.47$ )	5.97 ( $\pm 0.71$ )	20 ( $\pm 2.16$ )
ECC-U-10	99.19 ( $\pm 1.40$ )	9.87 ( $\pm 0.63$ )	6.35 ( $\pm 0.47$ )	19 ( $\pm 3.56$ )

However, with a further increase in UEA contents from 6%, compressive strength slightly decreased, reaching 98.56 MPa and 99.19 MPa at 8% and 10% contents of UEA, respectively. This indicates that in mixes with higher UEA, the presence of unreacted or

partially reacted UEA did not contribute to strength similar to the main hydration products, leading to a decrease in cube compressive strength.

Since UEA did not significantly affect the compressive strength, it indicates that HS-ECCs with UEA maintain sufficient strength for most construction applications requiring high strength. However, as UEA content increases beyond a certain limit, compressive strength decreases. Therefore, it is essential to select the optimal UEA content to avoid a significant reduction in compressive strength. While UEA can reduce autogenous shrinkage, its content must be carefully optimized to ensure that the compressive strength remains adequate for structural use.

#### 4.6. Tensile Strength

It was observed that UEA had a more significant impact on the tensile strength and strain than on cube compressive strength. Figure 10 and the accompanying Table 8 illustrate the effect of UEA on the tensile strength and strain of HS-ECCs after seven days. As the UEA content increased, the tensile strength initially increased while the tensile strain decreased. This improvement in tensile strength is attributed to enhanced hydration, which densifies the cement matrix, as also observed in compressive strength.

**Table 8.** Summary of the statistical analysis.

Parameters	Regression Analysis		Standardized Beta	Durbin-Watson	Confidence Interval (Slope)	Normality Test
	R <sup>2</sup>	p-Value				
Autogenous Shrinkage	0.981	<0.05	−0.991	2.677	[−47.751, 28.314]	0.381
Compressive Stress	0.015	>0.05	0.126	2.409	[−0.548, 0.629]	0.114
Tensile Stress	0.005	>0.05	0.069	1.623	[−0.542, 0.584]	0.316
Tensile Strain	0.796	<0.05	−0.892	1.607	[−0.523, −0.019]	0.329
Flow Diameter	0.992	<0.05	−0.996	1.499	[−5.502, −3.941]	0.333
Penetration Depth	0.995	<0.05	−0.997	2.627	[−0.317, −0.242]	0.689

For example, a mixture without UEA illustrated a tensile strength and tensile strain of 10.06 MPa and 8.40%, respectively. At a 6% UEA, the tensile strength increased to 12.25 MPa, while the tensile strain decreased to 4.81%. Further increasing the UEA content led to a reduction in the tensile strength and tensile strain. At 10% UEA, the tensile strength decreased to 10.16 MPa with a tensile strain of 5.01%. This further confirms that in mixtures with UEA, the unreacted or partially reacted UEA does not contribute as much as the primary hydration compounds, which leads to a reduction in tensile strength. At the same time, the low degree of hydration prevented a strong bond formation between the fibers and matrix, potentially causing a decrease in tensile strain. Additionally, the crack number decreased significantly with higher UEA contents. In an 80 mm section of the dog bone sample, the mixture without UEA had 34 cracks, which was reduced to 19 cracks at a 10% UEA.

The tensile properties of HS-ECCs are important features and are required for practical applications, especially in elements requiring high ductility. Despite a reduction in tensile performance with the increased UEA content, the tensile properties of HS-ECCs remain superior to those of conventional materials. This indicates that HS-ECCs can still be effectively used in real-world applications, provided that workability is properly managed and optimized.

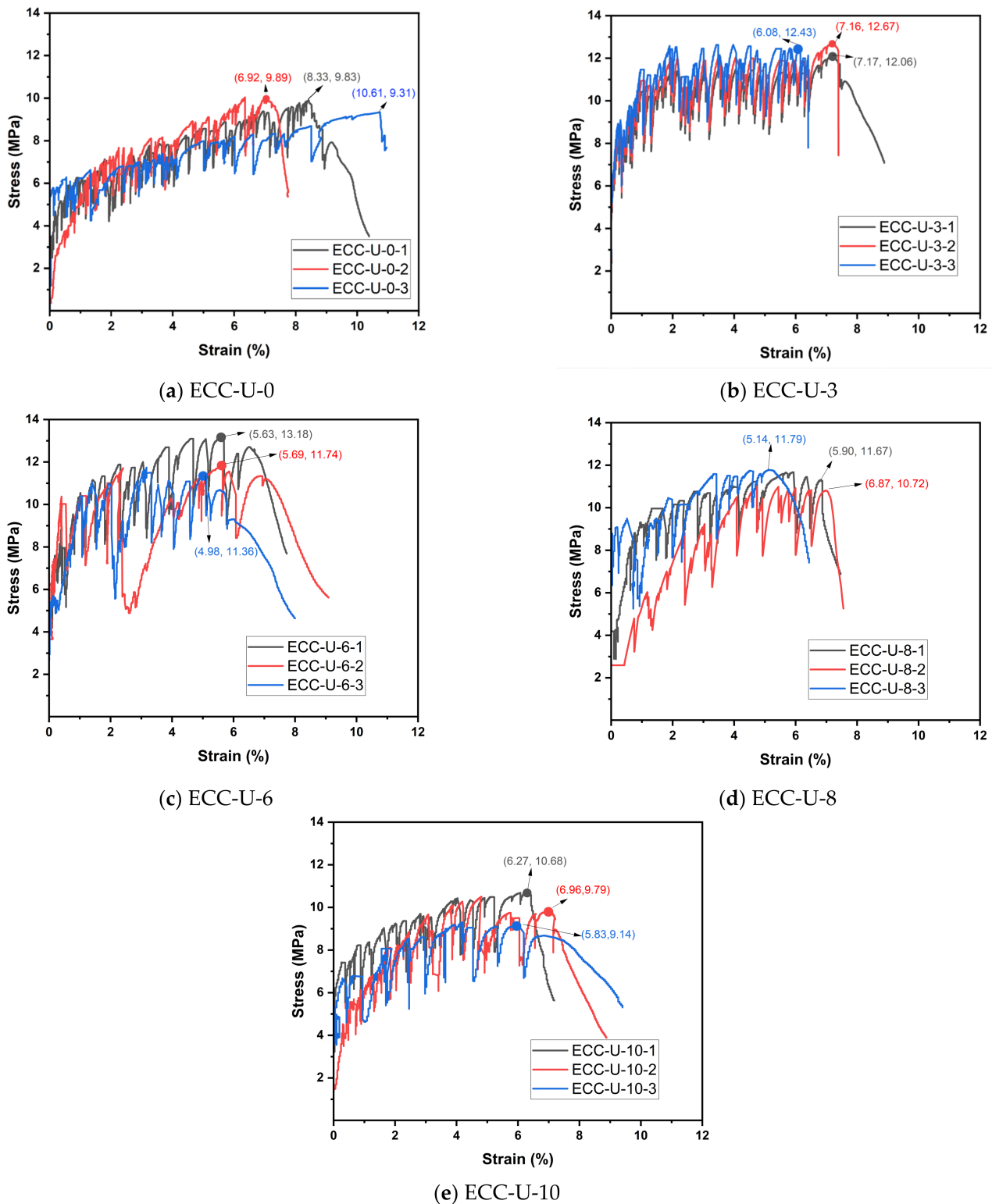


**Figure 10.** Tensile stress–strain curves of iron sand HS-ECCs at various UEA percentages.

### 5. Comprehensive Statistical Analysis of the Impact of UEA Content

A detailed statistical analysis was conducted to understand the role of UEA content on the properties of HS-ECCs. Regression analysis was performed to quantify and understand the relationships between UEA content, mechanical properties, workability, and shrinkage. This method accurately observes the impact of UEA content on these properties and provides informed decisions about mix design. Furthermore, to determine the strength and

direction of these relationships, standardized beta coefficients were utilized, which indicate the magnitude and impact of UEA on various properties.

The Durbin–Watson test was also used to check for autocorrelation to assess the reliability of the regression models and ensure the independence of residuals. This crucial step ensures that the results are accurate. The range within which the true influence of UEA on each property most likely falls was determined using the confidence interval for the slope, evaluating the accuracy and importance of the results. Finally, to confirm that the residuals had a normal distribution as required by linear regression assumptions, the Shapiro–Wilk normality test was performed. This test confirms that the models are correctly specified and supports the validity of the statistical findings. Collectively, these techniques were chosen to provide a thorough and accurate examination of the impact of UEA material on HS-ECCs. Table 8 summarizes the results of the statistical analysis.

For autogenous shrinkage, it can be concluded that UEA exhibits an excellent linear relationship with an  $R^2$  value of 0.981 and a  $p$ -value below 0.05. Furthermore, the standardized beta coefficient of  $-0.991$  confirms the negative impact of UEA on autogenous shrinkage. The Durbin–Watson analysis shows a value of 2.677, indicating no significant autocorrelation in the residuals, thus further validating the results. The 95% confidence interval for the slope is  $[-47.751, 28.314]$ , confirming a significant relationship. The  $p$ -value for the normality test is 0.381, suggesting normally distributed residuals.

Similarly, in the case of compressive strength, a weak correlation was observed with an  $R^2$  value of 0.015 and  $p > 0.05$ , suggesting a minimal impact of UEA on compressive strength. The small standardized beta coefficient of 0.126 shows a minor positive effect. The Durbin–Watson statistic is 2.409, indicating no significant autocorrelation. The 95% confidence interval for the slope is  $[-0.548, 0.629]$ , with zero within this range; this again confirms the lack of statistical significance. The normality test results ( $p = 0.1149$ ) indicate that residuals are normally distributed. Similarly, tensile stress values showed a low positive correlation of 0.005. The standardized beta coefficient of 0.069 for UEA content shows a very weak positive impact. The Durbin–Watson statistic was 1.623, indicating mild positive autocorrelation in the residuals. The confidence interval for the slope ranged between  $[-0.542, 0.584]$ , with zero within this range; this again confirms the lack of statistical significance. The normality test ( $p$ -value = 0.316) confirms that the errors are likely normally distributed.

However, a very strong linear relationship with an  $R^2$  value of 0.796 was observed for tensile strain. This indicates that 79.62% of the variation in tensile strain is explained by UEA content. The standardized beta coefficient of  $-0.892$  represents a strong negative impact. The Durbin–Watson statistic of 1.607 suggests mild positive autocorrelation. The significant result of the negative correlation is confirmed by the confidence interval of the slope, with a range of  $[-0.523$  to  $-0.019]$ . The assumption is supported as the  $p$ -value of the normality test was 0.329.

Workability, assessed by flow diameter and penetration depth, showed a strong correlation with UEA content. It was observed that workability decreased significantly with an increase in UEA content. For flow diameter, an  $R^2$  value of 0.992 was noted, while for penetration depth, an  $R^2$  of 0.9948 was observed, indicating a significant correlation with UEA content. The standardized beta coefficients for flow diameter and penetration depth are  $-0.996$  and  $-0.997$ , respectively. These values indicate a powerful and negative impact of UEA content on both properties. The Durbin–Watson statistics values for flow diameter and penetration depth are 1.499 and 2.627, respectively, suggesting mild positive autocorrelation in the residuals. The confidence intervals for the slopes,  $[-5.502$  to  $-3.941]$  for flow diameter and  $[-0.317$  to  $-0.242]$  for penetration depth, verify that the negative relationships are significant. According to the normality test of residuals for both parameters (0.333 and 0.689 for flow diameter and penetration depth, respectively), these residuals are likely normally distributed.

The present study reveals that UEA content significantly affects critical material properties, primarily autogenous shrinkage, tensile strain, flow diameter, and penetration depth.

High  $R^2$  values from regression analysis confirm the linear relationship of these properties with UEA content, explaining most of the variability. Standardized beta coefficients revealed very significant impacts of UEA on autogenous shrinkage and workability. The results of the normality tests were reliable, thus validating the analysis of the models. These findings highlight the necessity of proper content control of UEAs in material engineering approaches aimed at optimizing material performance.

## 6. Multi-Scale Integrated Evaluation

To assess the impact of UEA on the autogenous shrinkage, workability, and mechanical properties of HS-ECCs, tests for fluidity and penetration depth were conducted to evaluate workability. In contrast, cube compressive strength and direct tensile strength tests were used to determine mechanical properties.

Figure 11 illustrates that the mixture without UEA exhibited high autogenous shrinkage, high consistency, a large flow diameter, and high tensile strain, with both tensile and compressive strengths falling within acceptable ranges. As the UEA content increased to 3%, a significant reduction in autogenous shrinkage and an increase in compressive strength were observed, while tensile strain, flow diameter, and consistency showed declines.

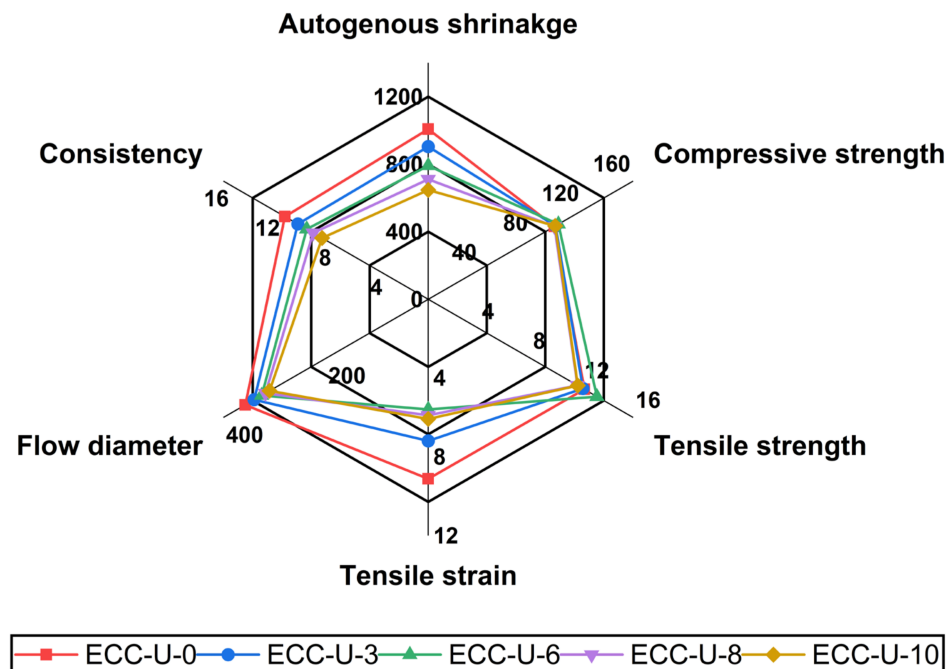


Figure 11. Multi-scale integrated evaluation under various UEA contents.

Further increasing the UEA content to 6% improved cube compressive and tensile strength, though workability continued to decrease. At higher UEA contents of 8% and 10%, reductions were noted across all parameters, including autogenous shrinkage, workability, and mechanical properties.

These findings suggest that while UEA effectively reduces autogenous shrinkage, it also negatively affects mechanical properties and workability, potentially limiting the practical use of HS-ECCs with a high UEA content. This highlights the importance of selecting the optimal UEA content to balance overall performance or optimizing mix proportions.

## 7. Conclusions

This study investigated the autogenous shrinkage, workability, and mechanical properties of HS-ECCs with iron sand. The influences of UEA content on setting time, autogenous shrinkage, flow diameter, penetration depth, cube compressive strength, tensile strength, and tensile strain were analyzed. Based on the obtained results, the following conclusions can be drawn.

(1) UEA significantly reduced autogenous shrinkage, with a maximum reduction of 40.66% observed at 10% UEA after 7 days. This demonstrates UEA's effectiveness in mitigating shrinkage, which is crucial for long-term durability.

(2) The incorporation of UEA led to decreased workability, as shown by reductions in the flow diameter and penetration depth. At 10% UEA, the flow diameter decreased from 357.5 mm to 310 mm, and the penetration depth reduced from 11.2 mm to 8.3 mm. This reduction indicates a need to balance the UEA content to maintain workability.

(3) The mixture with 10% UEA achieved the highest apparent density of 2594.68 kg/m<sup>3</sup>, within the normal concrete densities ranging from 1950 kg/m<sup>3</sup> to 2800 kg/m<sup>3</sup>.

(4) UEA had a minimal impact on the compressive strength. The strength slightly increased with up to 6% UEA, reaching 101.68 MPa, but decreased to 99.19 MPa at 10% UEA.

(5) UEA significantly influenced the tensile properties. At 3% UEA, the tensile strength increased to 12.38 MPa, while the tensile strain decreased to 6.80%. Further increases in the UEA content led to the reduced tensile strength and strain. Notably, the number of cracks decreased from 34 to 19 at 10% UEA content.

In conclusion, this research demonstrated that UEA effectively reduces autogenous shrinkage in HS-ECCs while impacting mechanical properties and workability. HS-ECCs have the potential to meet the demands of the construction industry. Incorporating iron sand lowers both the carbon footprint and cost, making HS-ECCs more feasible. A major challenge remains the high shrinkage strain associated with HS-ECCs, which needs to be addressed to enhance its suitability for civil engineering projects. Although UEA reduces shrinkage, it also negatively affects workability and tensile strain. Future research should focus on optimizing mix proportions to minimize shrinkage while improving workability and tensile properties. Exploring novel cement matrix composites with alternative binders, supplementary cementitious materials, or innovative additives could offer new opportunities to enhance durability, sustainability, and mechanical performance. Comprehensive testing at both the material and structural levels is essential to ensure these composites perform effectively under various service conditions. Additionally, the optimization of mixtures should be cost-effective to support large-scale civil engineering applications.

**Author Contributions:** Conceptualization, A.S.; data curation, A.S.; funding acquisition, L.L.; investigation, A.S., N.A. and Z.Z.; methodology, A.S. and Z.Z.; supervision, S.R. and L.L.; visualization, A.S.; writing—original draft, A.S.; writing—review and editing, S.R. All authors have read and agreed to the published version of the manuscript.

**Funding:** This research received no funding.

**Data Availability Statement:** The original contributions presented in the study are included in the article, further inquiries can be directed to the corresponding author.

**Conflicts of Interest:** The authors declare no conflicts of interest.

## Abbreviations

CEA	Calcium-oxide-based expansive agent
CSA	Calcium sulfoaluminate cement
E	Elastic modulus
ECC	Engineered cementitious composite
$f_{cu}$	Cube compressive stress
FST	Final setting time
$f_t$	Tensile stress
GGBFS	Ground granulated blast furnace slag
HS-ECC	High-strength engineered cementitious composite
HRWRA	High-range water-reducing admixture
IC	Internal curing
IOS	Iron sand
IST	Initial setting time

LVDT	Linear variable displacement transducer
MEA	Magnesium-oxide-based expansive agent
UEA	United Expanding Admixture
UHPC	Ultra-high-performance concrete
OPC	Ordinary Portland cement
PE	Polyethylene
SAP	Superabsorbent polymer
SF	Silica fume
SRA	Shrinkage-reducing admixture
s/b	Sand to binder
w/b	Water to binder
$\epsilon_t$	Tensile strain

## References

- Dong, Z.; Tan, H.; Yu, J.; Jiang, F. Using special coarse aggregate to enhance the tensile strain capacity of engineered cementitious composites. *Cem. Concr. Compos.* **2024**, *145*, 105347. [\[CrossRef\]](#)
- Yu, K.; Ding, Y.; Liu, J.; Bai, Y. Energy dissipation characteristics of all-grade polyethylene fiber-reinforced engineered cementitious composites (PE-ECC). *Cem. Concr. Compos.* **2020**, *106*, 103459. [\[CrossRef\]](#)
- Li, V.C. From micromechanics to structural engineering—The design of cementitious composites for civil engineering applications. *Struct. Eng. Earthq. Eng.* **1994**, *10*, 1–34.
- Cementitious, E.; For, C. Innovations Forum. *J. Mater. Civ. Eng.* **1997**, *9*, 1–6. [\[CrossRef\]](#)
- Zhu, J.-X.; Xu, L.-Y.; Huang, B.-T.; Weng, K.-F.; Dai, J.-G. Recent developments in Engineered/Strain-Hardening Cementitious Composites (ECC/SHCC) with high and ultra-high strength. *Constr. Build. Mater.* **2022**, *342*, 127956. [\[CrossRef\]](#)
- Leung, C.K.Y. Design criteria for pseudoductile fiber-reinforced composites. *J. Eng. Mech.* **1996**, *122*, 10–18. [\[CrossRef\]](#)
- Kanda, T.; Li, V.C. Practical design criteria for saturated pseudo strain hardening behavior in ECC. *J. Adv. Concr. Technol.* **2006**, *4*, 59–72. [\[CrossRef\]](#)
- Li, V.C.; Leung, C.K.Y. Steady-state and multiple cracking of short random fiber composites. *J. Eng. Mech.* **1992**, *118*, 2246–2264. [\[CrossRef\]](#)
- Ye, J.; Zhang, J.; Yu, J.; Yu, J.; Yu, K. Flexural behaviors of 3D printed lightweight engineered cementitious composites (ECC) slab with hollow sections. *Eng. Struct.* **2024**, *299*, 117113. [\[CrossRef\]](#)
- Yu, K.; Wang, Y.; Yu, J.; Xu, S. A strain-hardening cementitious composites with the tensile capacity up to 8%. *Constr. Build. Mater.* **2017**, *137*, 410–419. [\[CrossRef\]](#)
- Yu, K.; Li, L.; Yu, J.; Wang, Y.; Ye, J.; Xu, Q. Direct tensile properties of engineered cementitious composites: A review. *Constr. Build. Mater.* **2018**, *165*, 346–362. [\[CrossRef\]](#)
- Cai, Z.; Liu, F.; Yu, J.; Yu, K.; Tian, L. Development of ultra-high ductility engineered cementitious composites as a novel and resilient fireproof coating. *Constr. Build. Mater.* **2021**, *288*, 123090. [\[CrossRef\]](#)
- Dong, Z.; Tan, H.; Yu, J.; Liu, F. A feasibility study on engineered cementitious composites mixed with coarse aggregate. *Constr. Build. Mater.* **2022**, *350*, 128587. [\[CrossRef\]](#)
- Ding, Y.; Yu, K.; Li, M. A review on high-strength engineered cementitious composites (HS-ECC): Design, mechanical property and structural application. *Structures* **2022**, *35*, 903–921. [\[CrossRef\]](#)
- Kamal, A.; Kunieda, M.; Ueda, N.; Nakamura, H. Evaluation of crack opening performance of a repair material with strain hardening behavior. *Cem. Concr. Compos.* **2008**, *30*, 863–871. [\[CrossRef\]](#)
- Ghafari, E.; Ghahari, S.A.; Costa, H.; Júlio, E.; Portugal, A.; Durães, L. Effect of supplementary cementitious materials on autogenous shrinkage of ultra-high performance concrete. *Constr. Build. Mater.* **2016**, *127*, 43–48. [\[CrossRef\]](#)
- Xie, T.; Fang, C.; Mohamad Ali, M.S.; Visintin, P. Characterizations of autogenous and drying shrinkage of ultra-high performance concrete (UHPC): An experimental study. *Cem. Concr. Compos.* **2018**, *91*, 156–173. [\[CrossRef\]](#)
- Holt, E.E. Early age autogenous shrinkage of concrete. *VTT Publ.* **2001**, *446*, 2–184.
- Şahmaran, M.; Lachemi, M.; Hossain, K.M.A.; Li, V.C. Internal curing of engineered cementitious composites for prevention of early age autogenous shrinkage cracking. *Cem. Concr. Res.* **2009**, *39*, 893–901. [\[CrossRef\]](#)
- Maruyama, I.; Teramoto, A. Temperature dependence of autogenous shrinkage of silica fume cement pastes with a very low water-binder ratio. *Cem. Concr. Res.* **2013**, *50*, 41–50. [\[CrossRef\]](#)
- Ye, B.; Zhang, Y.; Han, J.; Pan, P. Effect of water to binder ratio and sand to binder ratio on shrinkage and mechanical properties of High-strength Engineered Cementitious Composite. *Constr. Build. Mater.* **2019**, *226*, 899–909. [\[CrossRef\]](#)
- Chen, Y.; Yao, J.; Lu, Z.; Leung, C.K.Y. Experimental study on the shrinkage reduction of high strength strain-hardening cementitious composites. *Cem. Concr. Compos.* **2019**, *104*, 103416. [\[CrossRef\]](#)
- Huang, H.; Ye, G. Examining the ‘time-zero’ of autogenous shrinkage in high/ultra-high performance cement pastes. *Cem. Concr. Res.* **2017**, *97*, 107–114. [\[CrossRef\]](#)
- Bentur, A.; Igarashi, S.; Kovler, K. Prevention of autogenous shrinkage in high-strength concrete by internal curing using wet lightweight aggregates. *Cem. Concr. Res.* **2001**, *31*, 1587–1591. [\[CrossRef\]](#)

25. Folliard, K.J.; Berke, N.S. Properties of high-performance concrete containing shrinkage-reducing admixture. *Cem. Concr. Res.* **1997**, *27*, 1357–1364. [[CrossRef](#)]
26. Ragalwar, K.; Heard, W.F.; Williams, B.A.; Ranade, R. Significance of the particle size distribution modulus for strain-hardening-ultra-high performance concrete (SH-UHPC) matrix design. *Constr. Build. Mater.* **2020**, *234*, 117423. [[CrossRef](#)]
27. Mehdipour, I.; Khayat, K.H. Effect of shrinkage reducing admixture on early expansion and strength evolution of calcium sulfoaluminate blended cement. *Cem. Concr. Compos.* **2018**, *92*, 82–91. [[CrossRef](#)]
28. Yang, L.; Shi, C.; Wu, Z. Mitigation techniques for autogenous shrinkage of ultra-high-performance concrete—A review. *Compos. Part B Eng.* **2019**, *178*, 107456. [[CrossRef](#)]
29. Zhang, J.; Wang, Q.; Zhang, J. Shrinkage of internal cured high strength engineered cementitious composite with pre-wetted sand-like zeolite. *Constr. Build. Mater.* **2017**, *134*, 664–672. [[CrossRef](#)]
30. Sherir, M.A.A.; Hossain, K.M.A.; Lachemi, M. Development and recovery of mechanical properties of self-healing cementitious composites with MgO expansive agent. *Constr. Build. Mater.* **2017**, *148*, 789–810. [[CrossRef](#)]
31. Musiał, M.; Lichołai, L. Multi-faceted analysis of phase-change composite intended for autonomous buildings. *Materials* **2024**, *17*, 2604. [[CrossRef](#)] [[PubMed](#)]
32. Zhang, Z.; Shrestha, A.; Cai, Z.; Ahmad, N.; Yu, K.; Li, L. Development of high-strength engineered cementitious composites using iron sand: Mechanical and shrinkage properties. *J. Build. Eng.* **2024**, *95*, 110272. [[CrossRef](#)]
33. Zhang, N.; Tang, B.; Liu, X. Cementitious activity of iron ore tailing and its utilization in cementitious materials, bricks and concrete. *Constr. Build. Mater.* **2021**, *288*, 123022. [[CrossRef](#)]
34. Shettima, A.U.; Hussin, M.W.; Ahmad, Y.; Mirza, J. Evaluation of iron ore tailings as replacement for fine aggregate in concrete. *Constr. Build. Mater.* **2016**, *120*, 72–79. [[CrossRef](#)]
35. Han, F.; Li, L.; Song, S.; Liu, J. Early-age hydration characteristics of composite binder containing iron tailing powder. *Powder Technol.* **2017**, *315*, 322–331. [[CrossRef](#)]
36. Wang, Z.; Bai, E.; Huang, H.; Wang, T.; Sun, H. Study on the electromagnetic property and microwave heating efficiency of concrete with magnetite aggregate. *Constr. Build. Mater.* **2022**, *342*, 128080. [[CrossRef](#)]
37. Aslani, F.; Asif, Z. Properties of ambient-cured normal and heavyweight geopolymer concrete exposed to high temperatures. *Materials* **2019**, *12*, 740. [[CrossRef](#)]
38. Lotfi-Omran, O.; Sadrumontazi, A.; Nikbin, I.M. A comprehensive study on the effect of water to cement ratio on the mechanical and radiation shielding properties of heavyweight concrete. *Constr. Build. Mater.* **2019**, *229*, 116905. [[CrossRef](#)]
39. Wang, D.; Che, J.; Liu, H.; Chin, S.C. Enhanced ductility and toughness of desert sand engineered cementitious composites. *Buildings* **2023**, *13*, 1538. [[CrossRef](#)]
40. Kumar, H.; Saini, B. Behaviour of engineered cementitious composite (ECC) with utilization of waste materials: A review. *Mater. Today Proc.* **2023**, *93*, 310–314. [[CrossRef](#)]
41. GB/T 1346-2011; Test Methods for Water Requirement of Normal Consistency, Setting Time and Soundness of the Portland Cement. China Building Materials Academy: Beijing, China, 2011.
42. ASTM C1698-09-2014; Standard Test Method for Autogenous Strain of Cement Paste and Mortar. ASTM International: West Conshohocken, PA, USA, 2019.
43. JGJ/T70-2009; Standard for Test Method of Basic Properties of Construction Mortar. Ministry of Housing and Urban-Rural Development: Beijing, China, 2009.
44. Ranade, R.; Li, V.C.; Stults, M.D.; Heard, W.F.; Rushing, T.S. Composite properties of high-strength, high-suctility concrete. *ACI Mater. J.* **2013**, *110*, 413–422. [[CrossRef](#)]
45. GB/T 50081-2019; Standard for Test Methods of Concrete Physical and Mechanical Properties. Ministry of Housing and Urban-Rural Development of the PRC: Beijing, China, 2019.
46. The Concrete Committee of the Japan Society of Civil Engineers. Recommendations for Design and Construction of High Performance Fiber Reinforced Cement Composites with Multiple Fine Cracks (HPFRCC). *Concr. Eng. Ser.* **2008**, *82*, 9–14. Available online: <http://www.jsce.or.jp/committee/concrete/e/index.html> (accessed on 28 June 2024).
47. Xie, L.; Liu, K. Properties and microstructure of Na<sub>2</sub>CO<sub>3</sub>-activated binders modified with Ca(OH)<sub>2</sub> and Mg(OH)<sub>2</sub>. *Materials* **2022**, *15*, 1687. [[CrossRef](#)] [[PubMed](#)]

**Disclaimer/Publisher’s Note:** The statements, opinions and data contained in all publications are solely those of the individual author(s) and contributor(s) and not of MDPI and/or the editor(s). MDPI and/or the editor(s) disclaim responsibility for any injury to people or property resulting from any ideas, methods, instructions or products referred to in the content.